Acta Crystallographica Section A
Foundations of Crystallography
ISSN 0108-7673

Received 17 July 2006
Accepted 4 December 2006

Tangled (up in) cubes

S. T. Hyde[a]* and G. E. Schröder-Turk[b]

[a]Department of Applied Mathematics, Research School of Physical Sciences, Australian National University, Canberra, ACT 0200, Australia, and [b]Institut für Theoretische Physik 1, Friedrich Alexander-Universität Nürnberg-Erlangen, Staudstrasse 7, 91054 Erlangen, Germany. Correspondence e-mail: stephen.hyde@anu.edu.au

The 'simplest' entanglements of the graph of edges of the cube are enumerated, forming two-cell $\{6, 3\}$ (hexagonal mesh) complexes on the genus-one two-dimensional torus. Five chiral pairs of knotted graphs are found. The examples contain non-trivial knotted and/or linked subgraphs [$(2, 2)$, $(2, 4)$ torus links and $(3, 2)$, $(4, 3)$ torus knots].

1. Introduction

The enumeration of the regular polyhedra dates back at least to Plato's *Academy*, where he introduces the Platonic polyhedra in his *Timaeus* (Plato, 1965). In the intervening millenia, our notion of polyhedra has broadened, to encompass Kepler's stellations of the five Platonic polyhedra and Coxeter's (and Petrie's) infinite polyhedra (Kepler, 1619; Coxeter, 1999; McMullen & Schulte, 1997). These examples reveal the shortcomings of too restrictive a definition of polyhedra; indeed, recent texts emphasize the difficulties of a sufficiently inclusive definition for polyhedra (Cromwell, 2001). Many examples deserve to be catalogued as significant relatives of Plato's regular examples; the question of just how many is perhaps dependent on our scientific motivation. Here we propose a simple hierarchy based on the topology of the (simplest) underlying manifold capable of carrying the (possibly knotted) network.

Knotted networks are of substantial interest to modern supra-molecular chemistry that has explored chemical realizations of simple graphs as molecules in some detail (Sauvage & Dietrich-Buchecker, 1999; Flapan, 2000). Chemists are now reporting metallo-organic crystals, whose supra-molecular structures exhibit complex catenation and threading, and contain knotted and linked subgraphs (Carlucci *et al.*, 2003*a*,*b*; Koch & Sowa, 2004; Fischer, 2004; Delgado-Friedrichs & O'Keeffe, 2005; Delgado-Friedrichs *et al.*, 2005). For example, a molecular crystal whose network topology is identical to that of the diamond network, but whose ambient isotopy is distinct, has been grown. Giant polymeric DNA networks display analogous complexity in the interweaving of individual DNA strands (Seeman & Lukeman, 2005). It seems likely that knotted structures will emerge in greater abundance as the polymeric nature of the crystalline ligands (that form the network edges) lengthens, due to the increased chance of intertwining of the extended ligands during self-assembly (just as the likelihood of a knotted polymeric chain increases dramatically with the degree of polymerization). Analysis of these knotted infinite networks is in its infancy. A reasonable starting point is to consider the simpler situation of a finite graph and knottings thereof.

1.1. Toroidal polyhedra

The exploration of toroidal polyhedra, containing holes, appears to be of recent interest. Some systematic studies of analogous examples to Archimedean polyhedra have been discussed in a now hard-to-find monograph (Stewart, 1970). Mathematicians have explored the concept of knotted graphs to a limited degree to date, though powerful (yet incomplete) invariants – derived from those of standard knots – are available to characterize their knotting (Conway & Gordon, 1983; Kauffman, 1989; Simon, 1987; Adams, 2002). So far, knottings of only the simplest graph – the *theta* graph with two degree three vertices and three edges – have been investigated in any detail (Wolcott, 1987; Litherland, 1989; Moriuchi, 2004). That work focused on the enumeration of knottings of the *theta* graph up to a certain complexity in a simple invariant of knots, the *crossing number* (the minimum number of edge crossings in a planar drawing of the graph). It seems preferable to us, however, to classify knotted embeddings of graphs in terms of the topological complexity of the lowest genus manifold capable of carrying the graph embedding.

It is helpful to clarify the terminology we will need. We consider a graph to be a connected network of (V) vertices and (E) edges. The graph topology is captured by (for example) a connectivity table that describes the vertices at either end of all edges. All graphs with the same topology are *isomorphic*. However, isomorphic copies may differ in their edge crossings, so that phantom moves, changing the crossing diagram, must be imposed to reveal the isomorphism between topologically equivalent graphs. The arrangement of under/over edge crossings is a feature of the *embedding* of the graph in space. Two isomorphic graphs that can be embedded in space to share the same arrangement of edge-crossings are *isotopic*: an ambient isotopy of the graph embedding is

sufficient to bring them into geometric coincidence. Thus, *isomorphs* of a given graph may have distinct knottings; we define *isotopes* to include all graph embeddings with the same knotting (*i.e.* geometric embeddings within an ambient isotopy). For convenience, we also allow chiral enantiomers of the embedding to lie within the same isotopic class and refer to right- and left-handed versions (referred to as + and − isotopes).

Platonic polyhedra tile the genus-zero sphere, whereas the stellated polyhedra tile multiple coverings of the sphere and the infinite polyhedra tile a handle-body with an unbounded genus (such as a triply periodic minimal surface). Modern derivations of the existence of Platonic polyhedra invoke Euler's relation; a topological equation that accords with the perspective we adopt here. The equation can be written

$$V - E + F = 2(1 - g), \qquad (1)$$

where V, E, F denote the number of vertices, edges and faces in a decoration of the surface of genus g, where all faces (minus their bounding edges) are open discs (known as a *two-cell embedding* of an oriented manifold without boundary). Regular polyhedra emerge as solutions provided $g = 0$. Note that this relation goes beyond a purely graph-theoretical perspective, as it includes the faces of the embedding. We view the two-cell embedding as a (potentially) knotted graph in three-dimensional Euclidean space ($\mathbb{E}^3$), as follows. The particular isotope of the graph is that induced by the embedding in $\mathbb{E}^3$ of the reticulated manifold. This route to construction of graph embeddings allows us to enumerate the isotopy of the graph of polyhedral edges – its knotting – *via* reticulation of the underlying two-manifold by the graph.

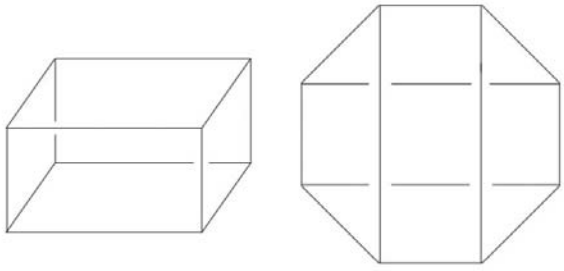

Figure 1
Two views of the unknotted (genus-zero) cube. The right-hand diagram is bounded by an octagonal Hamiltonian circuit of the cube.

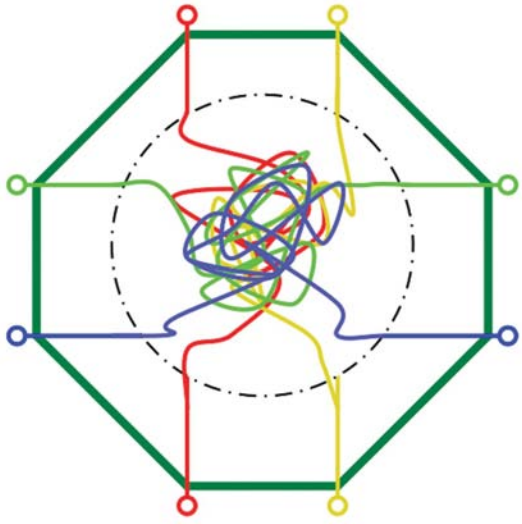

Figure 2
A knotted cube, with four tangled strands linking pairs of vertices in the bounding Hamiltonian (8-)cycle of the cube. Any internal tangle gives an isomorphic graph to the cube graph (the graph of cube edges).

Table 1
Knottedness of the 13 unit cells of the (6, 3) tiling that wrap onto the torus to form cube isomorphs.

In addition to one example of the conventional unknotted cube, five additional knotted isotopes emerge, labelled *A*-, *B*-, *C*-, *D*-, *E*-types. These emerge from various choices of lattice vectors of the (6, 3) Euclidean tiling, shown in Fig. 3.

Cube isotope	Lattice vectors	Images
Unknotted cube	{4, 0}, {0, 2}	Fig. 4
Isotope A^+	{4, 0}, {2, 2}	Fig. 8
Isotope A^+	{4, 2}, {0, 2}	Fig. 8
Isotope B^+	{8, 0}, {3, 1}	Fig. 12
Isotope B^-	{4, 4}, {3, 1}	Fig. 12
Isotope C^+	{4, 2}, {4, 0}	Fig. 15
Isotope C^-	{5, 1}, {2, 2}	Fig. 15
Isotope D^+	{6, 2}, {4, 0}	Fig. 18
Isotope D^-	{6, 2}, {2, 2}	Fig. 18
Isotope D^+	{0, 4}, {2, 2}	Fig. 18
Isotope E^+	{8, 0}, {5, 1}	Fig. 21
Isotope E^-	{4, 4}, {4, 2}	Fig. 21
Isotope E^+	{4, 4}, {1, 3}	Fig. 21

For example, the reticulation of a genus-zero sphere by the cube graph yields the well known (un)knotting of the cube graph, shown in Fig. 1. This isotope is characterized by six quadrilateral tiles covering the sphere, with three surrounding each vertex, giving the conventional Schläfli symbol for the cube, (4, 3).[1] Note that all cycles of the unknotted cube (4-, 6- and 8-cycles) are unknotted and pairs of (4-)cycles with disjoint edges form trivial unknotted two-component links.

We are concerned here with extension of that technique to the next-simplest oriented two-manifold: the (genus-one) torus. We call these examples *toroidal cubes*.

The identification of knotted embeddings that are topological cubes is readily done by checking the coordination sequence (Brunner & Laves, 1971) [or shell map (Aste *et al.*, 1996)] of the putative graph. The coordination sequence, $[i, j, k, \ldots]$, for a particular vertex origin describes the number of vertices displaced from the origin by shortest walk of length $1, 2, \ldots$. Among all five degree-three graphs with eight vertices (Brinkmann, 1996), only the graph of the cube edges has sequence [3, 3, 1] irrespective of the choice of vertex origin. An alternative identification procedure for cube-graph isomorphs containing an unknotted cycle passing through all vertices (a *Hamiltonian circuit*) can be done by inspection,

[1] We adopt the convention that $\{i, j\}$ and (i, j) refer to a network whose vertices form smallest cycles of length i with j edges coincident at each vertex. If i, j are enclosed between braces {, }, the network is geometrically embedded on an embedded two-dimensional surface in a Platonic form [*i.e.* flag transitive in the sense of Delaney–Dress tiling theory, with orbifold symmetry $\star 2ij$ (Conway & Huson, 2002)]. Otherwise, we denote the tiling (i, j).

checking that edges link third-neighbouring vertices along the Hamiltonian circuit, as in Fig. 2. Evidently, knotted varieties of the cube contain tangles of arbitrary complexity between the four internal edges within the Hamiltonian boundary (Fig. 2).

1.2. Regular cubes

Enumeration of *regular* reticulations of the torus has been explored to some extent. An exhaustive list of 'regular' two-cell complexes (tilings that fulfil the conditions required for Euler's relation to hold) has been published (Conder & Dobsanyi, 2001; Lijnen & Ceulemans, 2005). That definition is, however, very restrictive, as it demands that the topological symmetries of the reticulation (the group of automorphisms of the edges on the manifold) contain the group of automorphisms of the manifold itself as a normal subgroup. We relax that somewhat and require only that the two-cell embedding contains *topologically* identical vertices, edges and faces. In other words, we require that all faces of the two-cell embedding are of the same order, in addition to all vertices having the same degree. The question of symmetries of resulting embeddings in $\mathbb{E}^3$ is deferred to a later stage.

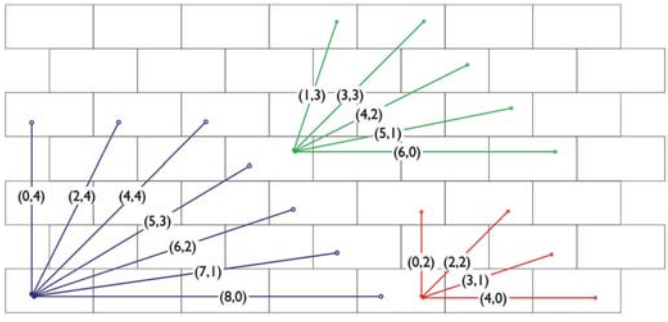

Figure 3
The (6, 3) tiling, drawn as the rectangular 'brick' tiling. Among all possible lattice vectors, we choose those that connect vertices to form graph cycles of length 8 (blue vectors), 6 (green) and 4 (red). The lattice vectors are labelled with their Cartesian vectors, where each brick is of (x) width 2 units and (y) height 1 unit.

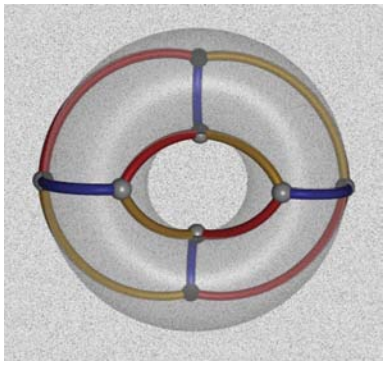

Figure 4
Embedding of the standard (unknotted) cube isotope on the torus. The minimal embedding of this isotope is on the sphere.

We note that this generous constraint on regularity is nevertheless sufficiently narrow to admit only the five Platonic polyhedra as regular genus-zero polyhedra.

We use this technique to explore possible knotted variants of the best known Platonic polyhedron: the cube.

2. Enumeration of toroidal cubes

The universal cover of any tiling of the torus is a two-periodic tiling of $\mathbb{E}^2$. Clearly, all isotopes of the cube share the standard features of the Platonic cube: eight vertices, all of degree three. We form reticulations of the torus that are topological cubes according to the following route. Since our definition of regularity demands equal polygons for all tiles and the degree

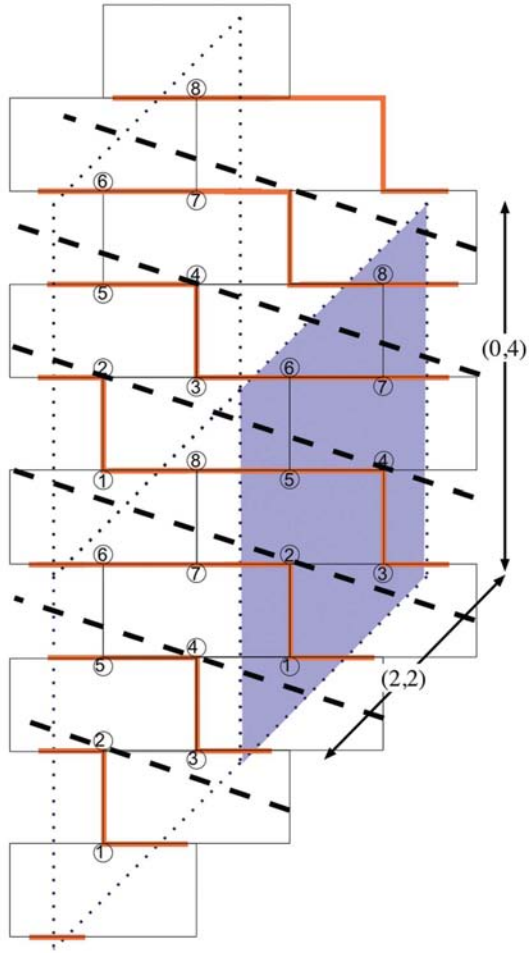

Figure 5
Example of a two-periodic planar pattern that defines a torus reticulation by the (6, 3) tiling, containing eight vertices within each unit cell, labelled by circled integers 1, 2, . . . , 8. Three adjacent rhombohedral unit cells are drawn bounded by dotted parallelograms. A pair of lattice vectors defining the unit-cell edges are labelled by their Cartesian position vectors (0, 4) and (2, 2). The parallel meanders (orange lines) represent a single Hamiltonian 8-cycle of the compact genus-one graph (127634581 . . .). The dashed lines indicate the average pitch of the meanders; their intersections with unit-cell edges determine the homotopy of this 8-cycle. In this example, dashed lines intersect the (0, 4) edges thrice and the (2, 2) edges twice. This cycle is therefore a knotted loop with homotopy (3, 2) on the torus; a trefoil.

of the tiling is equal to three, all faces must be hexagons [*i.e.* the (6, 3) tiling of the Euclidean plane]. First, embed the (6, 3) tiling in $\mathbb{E}^2$. For our purposes, it is sufficient and convenient to use a brick tiling, with bricks two units wide and one unit high. In that configuration, vertices of the (6, 3) tiling have positions $(x, y) = (2p + \mathrm{mod}\,2[q], q)$, where $p \in \{0, 1, 2, \ldots, i\}$ and $q \in \{0, 1, 2, \ldots, j\}$. The integers a and b define gluing vectors of the torus: the points (x, y), $(x + a, y)$, $(x, y + b)$ and $(x + a, y + b)$ *etc.* coincide on the torus. The 'gluing vector' (a, b) then defines the fundamental homotopic loops (or collars) of the torus. Provided gluing vectors are lattice vectors of the (6, 3) tiling, a multiple cover of the torus with identically positioned tiles on each cover results.

All cycles of the cube graph traverse four, six or eight vertices only. Though longer closed walks are possible on the cube graph (by appending additional loops), we confine this analysis to cycles of length four, six and eight only, to constrain the enumeration to manageable proportions. This constraint restricts allowed lattice vectors considerably. The number of admissible lattice vectors is equal to the sum of entries in the coordination sequence for the (6, 3) network at positions 4, 6 and 8; *viz* 12 + 18 + 24. We reduce those vectors to those with non-negative entries, giving four, five and seven distinct lattice vectors for cycles of length four, six and eight, respectively, shown in Fig. 3. Any pair of these lattice vectors can be used to define a torus whose cycles are of the requisite length. Among those pairs, we select only those containing eight vertices within a single unit cell. That constraint leaves us with 20 pairs of lattice vectors, leading to 20 geometrically distinct tori.

Among those 20 solutions, seven are not cube isomorphs (since their coordination sequences do not match that of the

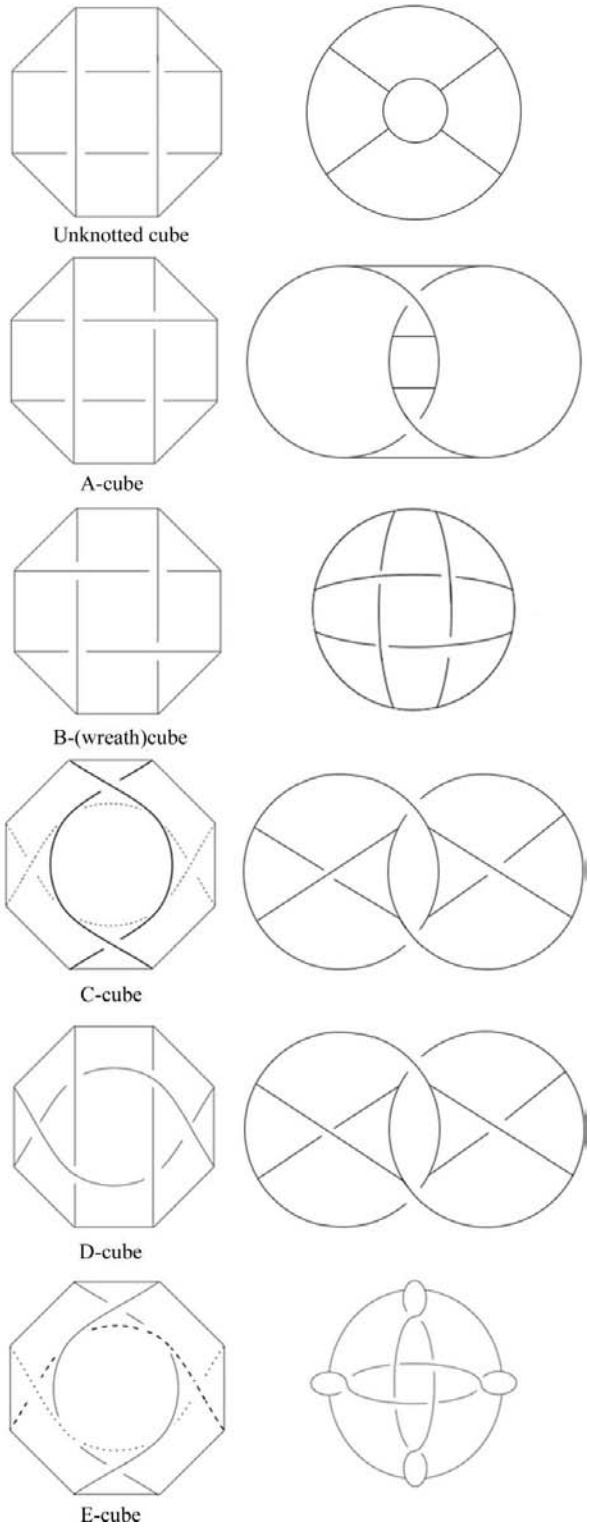

Figure 6
The six simplest embeddings of the graph of edges of the cube. The unknotted cube tiles the (genus zero) sphere; knotted cubes $A - E$ tile the genus-one torus. The latter graph embeddings are all chiral, we show here only one of the enantiomers. The left column shows images of all isotopes bounded by an unknotted Hamiltonian circuit; the right column displays the knotted graphs with minimal crossing number.

Figure 7
Vessel #2, a fibreglass and acrylic sculpture realized by Robert Owen (2003). Image courtesy of Sherman Galleries, Sydney.

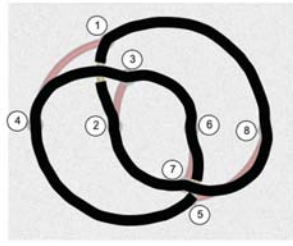

Figure 8
Isotope A with the Hopf link highlighted (red and blue cycles).

cube). Of the remaining 13 topological cubes, one turns out to be an embedding of the standard (unknotted) cube on the torus (Fig. 4). The remaining 12 are novel genus-one isotopes of the cube. How many of these are distinct isotopes? We use the isotopic invariants for knotted graphs described by Kauffman, namely, the standard knot and link invariants formed by all possible cycles of the graph (Kauffman, 1989). These embed on the torus as simple (unbranched) knots and links with characteristic homotopic signatures, described below. This technique is sufficient to distinguish distinct achiral isotopes (though it typically fails to distinguish chiral enantiomers), provided they are characterized by distinct embedded knots and/or links as subgraphs. Where embeddings share an identical suite of knots or links, but display

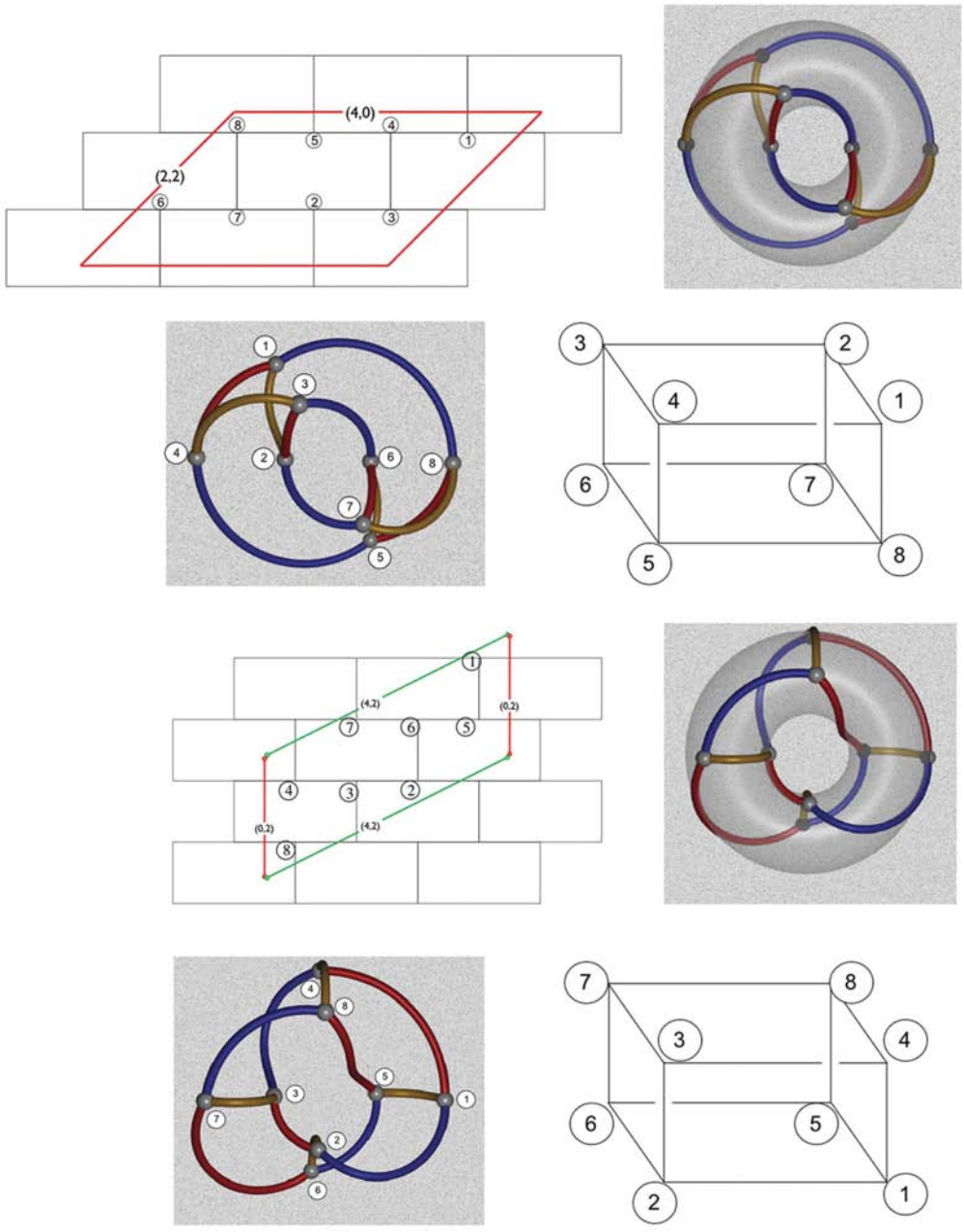

Figure 9
The *A*-type cube; the simplest cube tangle. The top left image shows the fragment of the (6, 3) tiling of the Euclidean plane and the unit cell with lattice vectors (4, 0) and (2, 2) (see Fig. 3), containing eight degree-three vertices (labelled 1–8). The embedding that emerges by identifying translation-equivalent points, forming a torus, and then embedding the edges in three-dimensional Euclidean space is shown to the right. Second row, left: Vertex labelling in the toroidal embedding corresponding to those in the (6, 3) tiling. Right: Alternative view of the type-*A* isotope as the classic 'impossible' cube, which is impossible only if it is assumed to reticulate a sphere! Third, fourth rows: Equivalent images resulting from the the (6, 3) tiling of the Euclidean plane and the unit cell with lattice vectors (4, 2) and (0, 2). This wraps on the torus to form slightly different unknotted cycles to the previous case (*cf.* Table 2), however, it gives an equivalent isotope.

Table 2
Distinct isotopes of the cube graph that embed on the genus one torus, ranked from least to most tangled.

The homotopies of the cycles on the torus are listed in the same order as the torus gluing vectors (lattice vectors). All cycles of length eight (Hamiltonian circuits) and links containing a pair of 4-cycles are listed. Cycles of length six are listed only for the knotted examples: four 6-cycles in the *E*-type isotope. Blank entries in the knot type column signify that the relevant knots/links are trivial (*i.e.* unknotted).

Isotope name	Lattice vectors	Cycle(s)	Homotopy	Knot type
A	(4, 0), (2, 2)	12345678	(2, 1)	
		12367854	(1, 1)	
		12763458	(1, 2)	
		12785634	(2, 1)	
		14327658	(1, 1)	
		14563278	(1, 2)	
		(1278)(3654)	(1, 1)(1, 1)	Hopf (2_1^2) link
		(1854)(2367)	(0, 1)(0, 1)	
		(1234)(5678)	(1, 0)(1, 0)	
A	(4, 2), (0, 2)	12673485	(3, 1)	
		15623784	(1, 1)	
		12658734	(1, 0)	
		15678432	(1, 0)	
		14873265	(1, 1)	
		12376584	(1, 0)	
		(1234)(5678)	(1, 1)(1, 1)	Hopf (2_1^2) link
		(1485)(2376)	(0, 1)(0, 1)	
		(1562)(3487)	(1, 0)(1, 0)	
B	(4, 4), (3, 1)	12345678	(0, 1)	
		12367854	(1, 0)	
		12763458	(1, 0)	
		12785634	(4, 1)	
		14327658	(1, 0)	
		14563278	(1, 0)	
		(1278)(3456)	(1, 0)(1, 0)	
		(1432)(8567)	(1, 0), (1, 0)	
		(2367)(1854)	(2, 1)(2, 1)	4_1^2 link
C	(5, 1), (2, 2)	12345678	(1, 2)	
		12387456	(1, 1)	
		12543876	(1, 1)	
		12567438	(1, 1)	
		16523478	(1, 1)	
		16745238	(3, 2)	Trefoil (3_1) knot
		(1678)(2543)	(1, 1)(1, 1)	Hopf (2_1^2) link
		(1256)(7834)	(1, 0)(1, 0)	
		(3812)(4765)	(1, 1)(1, 1)	Hopf (2_1^2) link
D	(0, 4), (2, 2)	12345678	(0, 1)	
		12367854	(3, 1)	
		12763458	(3, 2)	Trefoil (3_1) knot
		12785634	(0, 1)	
		14327658	(3, 1)	
		14563278	(3, 2)	Trefoil (3_1) knot
		(1432)(8567)	(1, 0)(1, 0)	
		(2781)(3654)	(1, 1)(1, 1)	Hopf (2_1^2) link
		(3276)(1854)	(2, 1)(2, 1)	4_1^2 link
E	(4, 4), (4, 2)	17654328	(0, 1)	
		17632845	(1, 1)	
		17236548	(1, 1)	
		17284365	(4, 3)	8_{19} knot
		15672348	(1, 1)	
		15436728	(1, 1)	
		172845	(3,2)	Trefoil (3_1) knot
		284367	(3,2)	Trefoil (3_1) knot
		172365	(3,2)	Trefoil (3_1) knot
		184365	(3,2)	Trefoil (3_1) knot
		(3276)(1548)	(2, 1)(2, 1)	4_1^2 link
		(7281)(6345)	(1, 1)(1, 1)	Hopf (2_1^2) link
		(1567)(4823)	(1, 1)(1, 1)	Hopf (2_1^2) link

unknotted cycles (trivial knots) with distinct homotopic signatures, we must look further. Thus, we first bundle the 12 solutions into distinct isotopy classes and then investigate the possibility of chiral versions within each class.

All examples are – by construction – torus embeddings, so that the possible knots and links are torus knots, readily characterized by their homotopy on the torus. Those data describe the homotopic winding of each cycle around the torus with respect to the basis vectors of the fundamental group of the torus. Each cycle unfolds to a meandering path in the universal cover of the torus reticulation. The average pitch of the meander can be determined visually from its crossings with the unit-cell boundaries that make up a single torus. A typical example is shown in Fig. 5. This example – the Hamiltonian cycle 127634581 on isotope *D* – forms a cycle of homotopy (3, 2) with respect to the torus defined by an ordered pair of lattice vectors (0, 4) and (2, 2), corresponding to the average pitch of the meander 127634581 . . . in the universal cover. The (3, 2) torus knot is the simplest non-trivial knot: the trefoil (Adams, 2002). The corresponding knot on the cube isotope *D* is illustrated in Fig. 19. Cycles with homotopy (c, d) form non-trivial knots provided the fraction c/d is not an integer. Tangled links can also be identified from their homotopy type: *n*-component links on the torus necessarily comprise

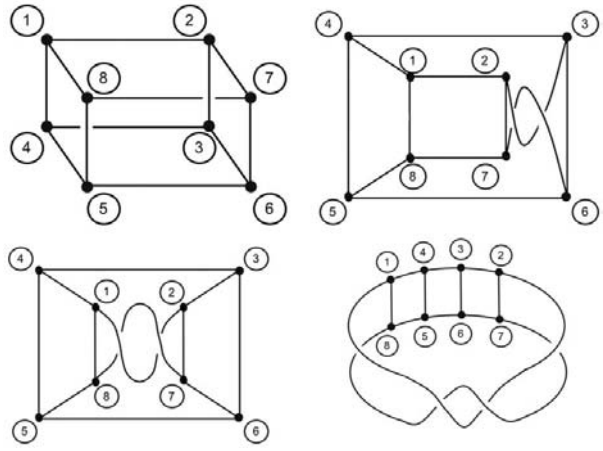

Figure 10
Deformation (an ambient isotopy) of the embedding of the *A*-type isotope shown in Fig. 8 to form the chiral four-rung twisted ladder.

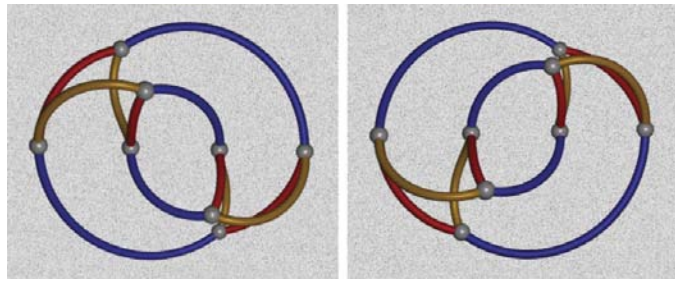

Figure 11
Left- and right-handed A^+ and A^- isotopes.

homotopically equivalent cycles; (ne, nf), where e and f are non-zero (Adams, 2002).

Using this approach, we have determined the knot class for all cycles and links in tangled cubes – constrained to arise from (6, 3) tilings on the torus, with maximum cycles of length eight – that reticulate the torus. The complete set of cycles on cube isomorphs comprises six Hamiltonian cycles (of length eight), 16 6-cycles (including four Petrie polygons of the cube) and six 4-cycles. Multiple cycles are links, provided the edges within distinct cycles are disjoint. Admissible links for cube isomorphs are the three pairs of 4-cycles with disjoint edges (corresponding to the edges of opposite faces in the unknotted cube). We have determined the knot class from the meander homotopy for all distinct 8-cycles, 6-cycles and links formed by pairs of 4-cycles.

The suite of non-trivial knots and links for the 12 novel cube isotopes have been exhaustively determined (Table 1). Their cycle homotopies fall into six distinct classes. Two of those share the same non-trivial knot and have slightly different unknotted Hamiltonian circuits, forming equivalent isotopes in three-dimensional Euclidean space, $\mathbb{E}^3$. We therefore find five distinct genus-one isotopes (plus chiral enantiomers), according to Kauffman's invariant described above. These are compared with the conventional (unknotted) cube in Fig. 6.

Two knots are present in these tangled cubes: the trefoil knot [homotopy class (2, 3), Alexander-Briggs symbol 3_1] and

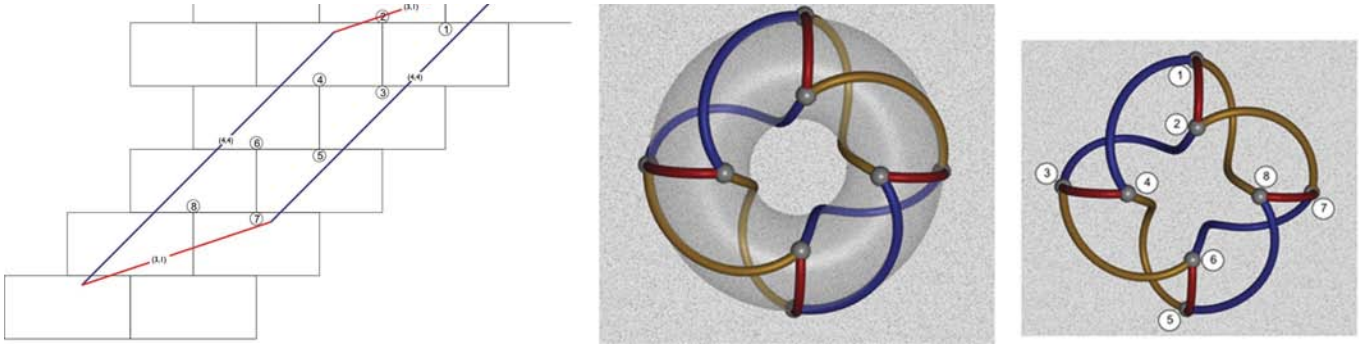

Figure 12
Isotope *B*, the 'wreath cube'.

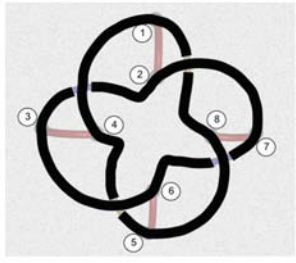

Figure 13
The *B*-type cube, the wreath cube, with the cycles making up the 4_1^2 link highlighted.

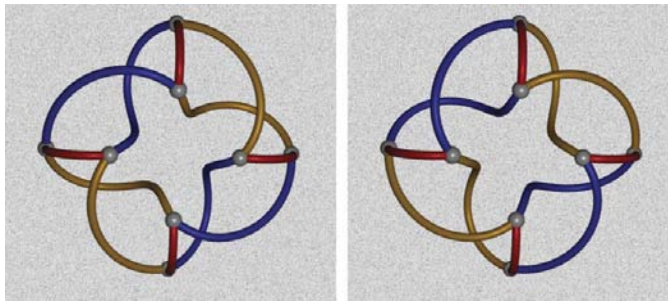

Figure 14
Left- and right-handed wreath cubes (B^+, B^- isotopes).

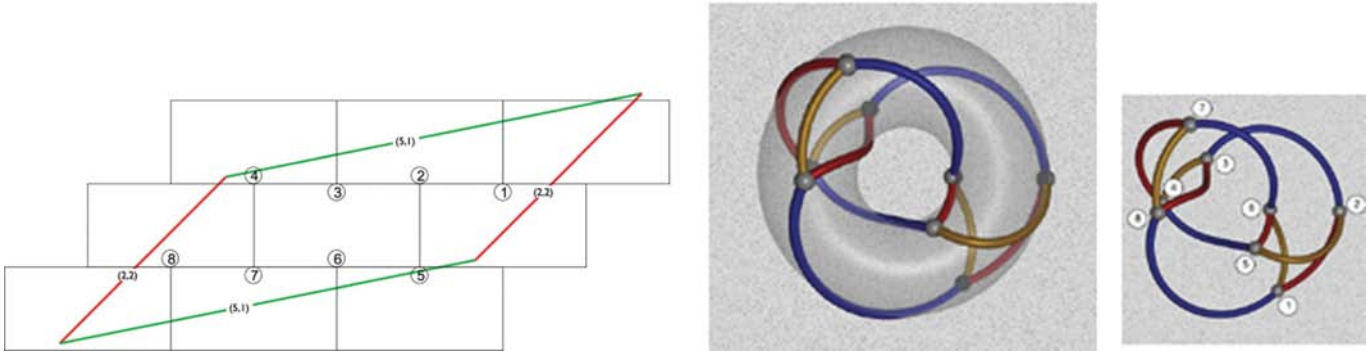

Figure 15
The *C*-type cube.

the 8_{19} knot [homotopy class (3, 4)]. In addition, two distinct links are found: the Hopf link [2_1^2, homotopy class (2, 2)] and the 4_1^2 link [homotopy class (2, 4) on the torus]. (All 4-cycles are unknotted.) The cycles are labelled by their vertices following the vertex numbering displayed in the figures in the main text. The data are collected in Table 2.

3. Three-dimensional embeddings of tangled cubes

The problem of finding a canonical embedding for these toroidal polyhedral graphs does not have a clear solution. The issue is in stark contrast to the analogous problem for isomorphs of crystalline graphs in $\mathbb{E}^3$: in most cases, barycentric embeddings provide a simple solution, choosing a metric embedding of the 'equilibrium placement' (Delgado-Friedrichs & O'Keeffe, 2003) in a simple cubic unit cell. We can adapt the equilibrium placement idea to our case, to find an embedding of the (6, 3) graphs in $\mathbb{E}^2$; namely the geometrically regular {6, 3} (Platonic) net. That placement gives the barycentric coordinates of the net on the flat torus (whose universal cover is $\mathbb{E}^2$). The flat torus is not embeddable in $\mathbb{E}^3$ without metric distortion; nevertheless, we can proceed further with that idealization to give an embedding. For convenience only, we have chosen a standard embedding of the torus whose (orthogonal) generators of the fundamental group [(1, 0) and (0, 1)] embed in $\mathbb{E}^3$ such that one period is twice the length of the other. We have adopted that convention here to allow for comparable embeddings of all cube isotopes. The resulting images, both on the torus and removed from the torus without further spatial deformation, are displayed with edges consistently coloured in one of three colours (gold, red and blue) among the figures mentioned below.

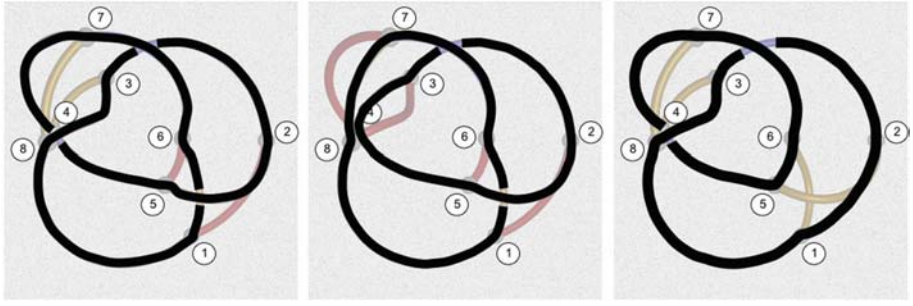

Figure 16
Left to right: The trefoil knot contained in a Hamiltonian circuit (16745238) of the *C*-type isotope and a pair of Hopf links (*cf.* Table 2).

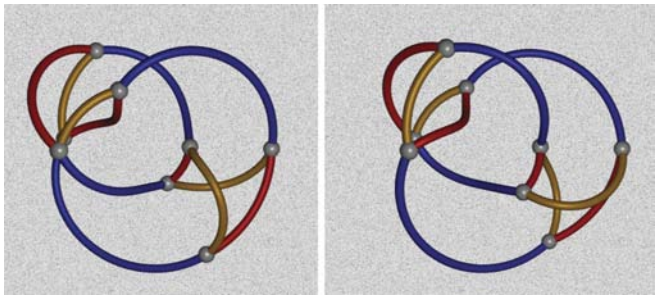

Figure 17
C^+ and C^- isotopes of the cube.

3.1. Isotope *A*

Among all the cube graphs that contain knots or links, one pair of examples, defined by the lattice vectors (4, 0), (2, 2) and (4, 2), (0, 2), contains only a single Hopf link. [The latter case contains an unknotted cycle of length eight slightly different to those listed in Table 2, with homotopy (3, 1). However, as explained below, this does not result in a distinct knotting in $\mathbb{E}^3$.] This isotope, labelled for convenience *A*-type, is the simplest knotted isotope. It can be drawn with two crossings, producing an 'impossible cube' to the untrained eye. It is a favourite motif for artists, psychologists and mystics.[2] A beautiful rendering of this isotope is a recent sculpture by the Australian artist, Robert Owen (Owen, 2003) (Fig. 7). This example is the simplest tangled isotope of the cube: a single phantom move, exchanging crossings, is sufficient to recover the conventional (genus-zero, untangled) cube. All cycles of this isotope are unknotted, while just a single pair of disjoint 4-cycles are linked, forming the Hopf 2_2^1 link [a (2, 2) link on the torus, with a pair of interwoven cycles of homotopy (1, 1) each]. This link is highlighted in Fig. 8. *A*-type isotopes include two of the six distinct embeddings distinguished by their cycle homotopies on the torus (Table 2). The pair share the same link but have distinct – unknotted – Hamiltonian cycle homotopies. These differences are not manifested as distinct isotopes in $\mathbb{E}^3$. Toroidal reticulations, unrolled into $\mathbb{E}^3$, of the pair as well as alternative Schlegel diagrams, to be read as embeddings in $\mathbb{E}^3$, are shown in Fig. 9. The possibility of *topological chirality* (Simon, 1987) of isotope *A* – with non-superimposable mirror images regardless of the geometry of the isotope – requires checking. (Note that the unknotted cube is topologically achiral). Simple deformation of the isotope geometry allows us to draw this isotope as a four-rung twisted cylinder (see Fig. 10), proven by Simon to be topologically chiral (Simon, 1987). Therefore, two distinct enantiomers of the *A*-type isotope occur, A^+ and A^-, drawn in Fig. 11.

3.2. Isotope *B*: the wreath cube

A second distinct isotope – the *B*-type isotope – of the cube is an elegant generalization of an alternating braid, with a crossing number of four. It embeds on the torus to give a

[2] The analysis of 'impossible figures' such as knots and braids has been noted previously (Cowan, 1982; Cerf, 2002), though the examples and approach canvassed elsewhere are related to thickened polyhedral edge structures, such as the Penrose tribar.

wreath-like pattern: we call this the *wreath* cube. Its universal cover and a simple Schlegel representation are shown in Fig. 12. Its Hamiltonian cycles and all 6-cycles are unknotted. One pair of 4-cycle links is knotted, forming the 4_1^2 link, a pair of torus cycles, each of homotopy (2, 1) (Fig. 13). It follows from the non-palindromic nature of the coefficients of the Jones polynomial of the 4_1^2 link that this link is topologically chiral (Adams, 2002). Therefore, isotope *B*, like the previous example, is chiral (see Fig. 14).

3.3. Isotope *C*

A third distinct cube isotope (Fig. 15) is the simplest example to contain knotted Hamiltonian circuits. It includes a trefoil (3_1) knot containing all eight vertices of the cube (Table 2, Fig. 16). Its minimal crossing number is four. All 6-cycles are unknotted. However, all three links formed by pairs of disjoint 4-cycles are non-trivial; forming two Hopf links and a 4_1^2 link. The presence of topologically chiral links (4_1^2) and the chiral trefoil knot establishes the existence of a pair of distinct chiral enantiomers, drawn in Fig. 17.

3.4. Isotope *D*

An additional distinct isotope of the cube graph, with crossing number four, is shown in Fig. 18. This isotope – *D*-type – contains a pair of knotted Hamiltonian circuits; both trefoils of the same handedness (Fig. 19); all 6-cycles are unknotted. It also includes a Hopf and a 4_1^2 link (*cf.* Table 2). The presence of these topologically chiral knots and links establishes the presence of an enantiomeric pair of *D*-type isotopes, drawn in Fig. 20.

3.5. Isotope *E*

This isotope, with (minimal) crossing number eight is shown in Fig. 21. It is the most tangled example among those enumerated here, with five knots and three links (Fig. 22). Its 4-cycles contain the same suite of links as those found in isotope *C*. Like *C*, a single Hamiltonian circuit is knotted; in this case, to form the chiral 8_{19} knot. This is the sole example to exhibit knotted 6-cycles: four of the sixteen 6-cycles form trefoils. The presence of these chiral knots proves that *E*-type

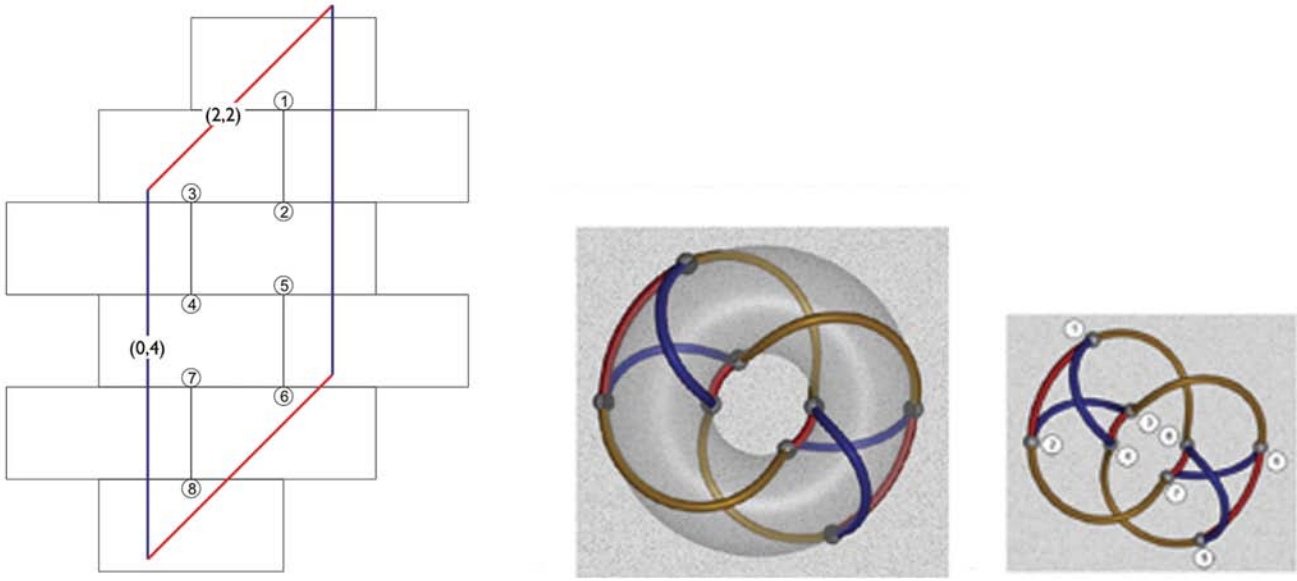

Figure 18
The *D*-type cube.

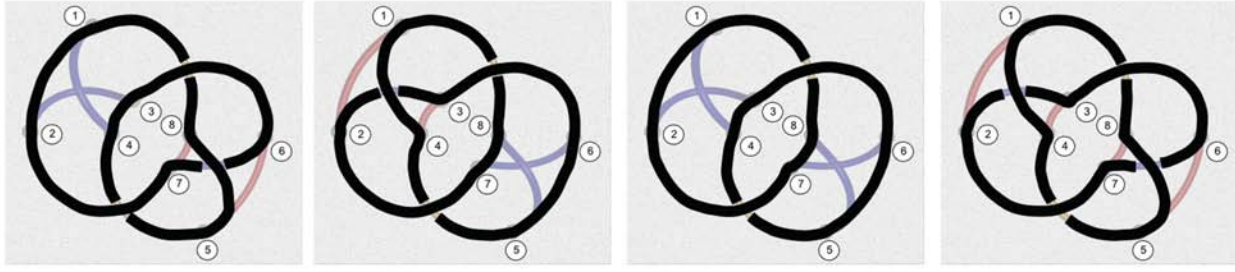

Figure 19
Left: the pair of like-handed trefoil knots found in the type-*D* isotope. Right: the Hopf and 4_1^2 links.

isotopes of the cube also exist in two enantiomeric forms regardless of the embedding, shown in Fig. 23.

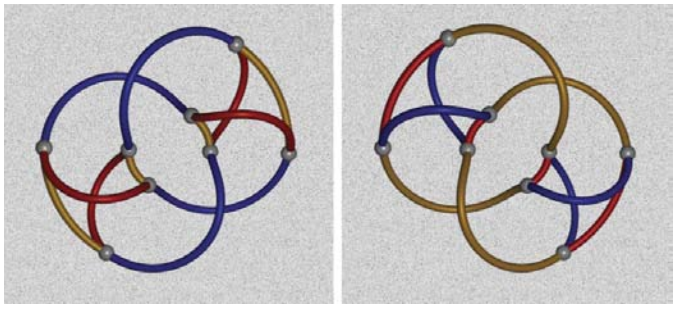

Figure 20
D^+ and D^- isotopes of the cube.

4. Extensions: infinite networks and other polyhedral knottings

Our primary goal here has been to explore the concept of generalized polyhedral edge graphs that result from reticulations of the genus-one torus. The implication of this work is that we can enumerate knotted polyhedral isotopes according to the topological complexity of the simplest manifold that carries the knotted graph. The technique is simply modified to detect toroidal isotopes of other Platonic polyhedra, though the combinatorics rapidly give large numbers of solutions. The approach furnishes relatively simple knottings of the cube, as anticipated by the topological constraints. Relaxing the constraint on the largest cycle length gives an infinite number of solutions whose edges wind around the torus in tighter loops. These cases will be analysed in a forthcoming paper

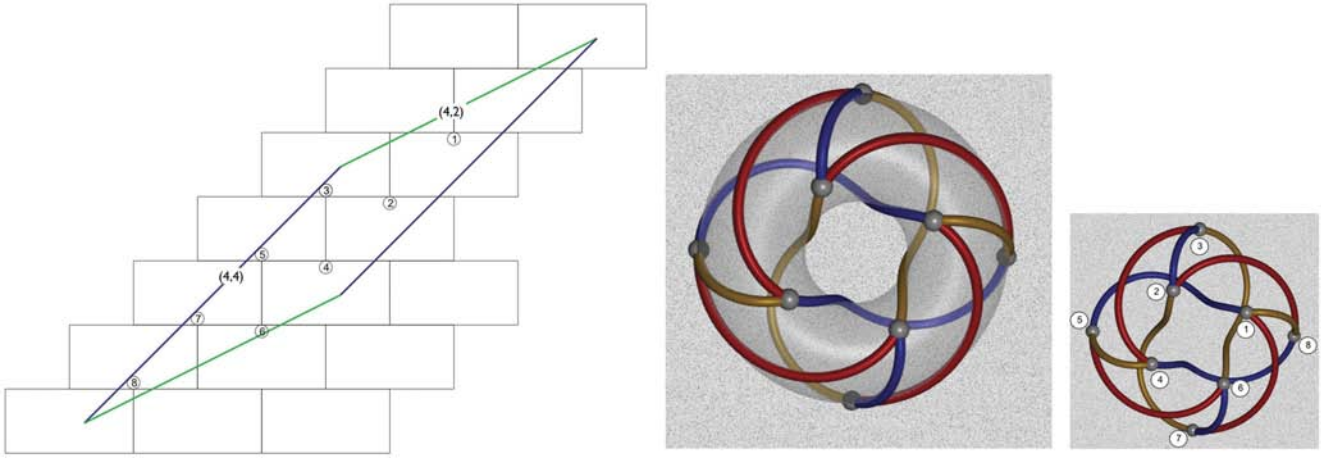

Figure 21
The *E*-type cube.

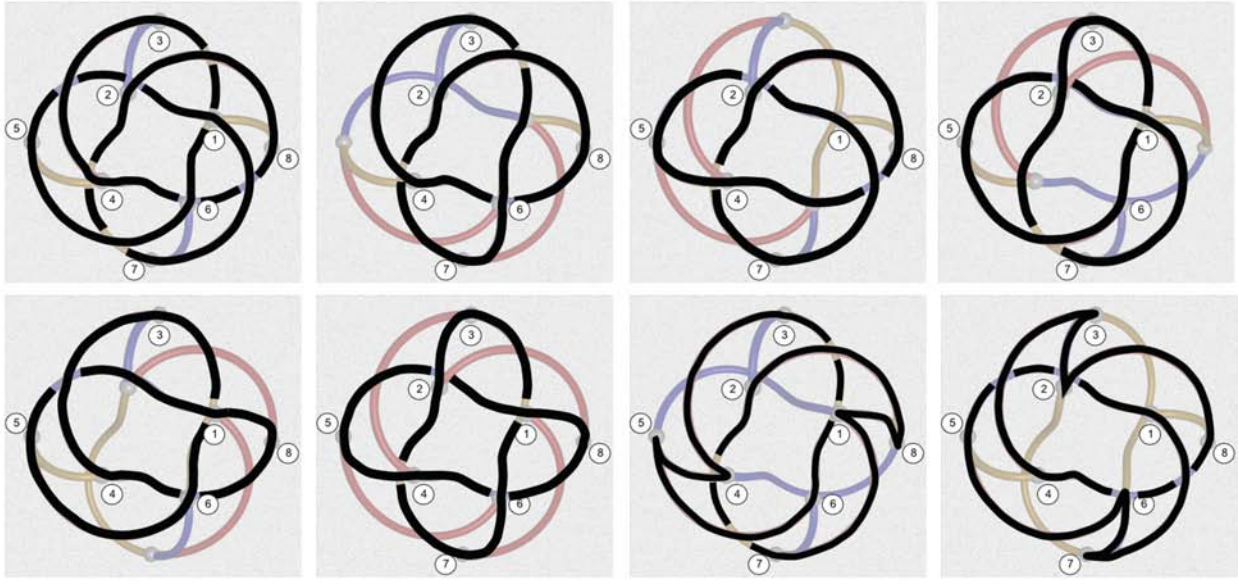

Figure 22
Top row: The chiral 8_{19} knot and three distinct trefoils highlighted within the *E*-type isotope. Bottom row: A fourth trefoil, a 4_1^2 link and a pair of Hopf links. Note that all trefoils are like-handed.

(Castle *et al.*, 2007). The technique can be extended to higher-genus tori. Some steps in that direction have been done already, en route to enumeration of 3-periodic nets *via* reticulations of 3-periodic minimal surfaces (TPMS), in the *EPINET* project (Ramsden *et al.*, 2005). Just as the glued two-dimensional Euclidean unit cells are genus-one tori, the glued three-dimensional cells of the TPMS used to date are all genus-three tori. All 3-periodic crystal nets generated *via* this method can therefore be reduced modulo their three distinct lattice vectors to form finite networks that reticulate the genus-three two-dimensional torus. Many thousand examples are therefore already implicitly derived (Hyde *et al.*, 2006). We plan to process those examples, finding distinct isotopes, in the near future. Finally, we note that the examples deduced here offer intriguing units for construction of three-periodic networks in $\mathbb{E}^3$. We reiterate that spatial realizations of toroidal cube isotopes in $\mathbb{E}^3$ are far from unique – an infinity of metric realizations of any isotope are possible. Indeed, all the

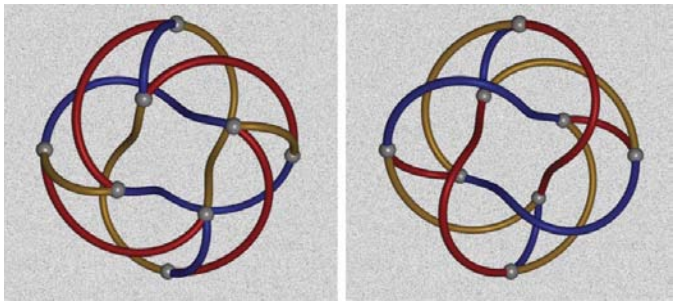

Figure 23
E^+ and E^- isotopes of the cube.

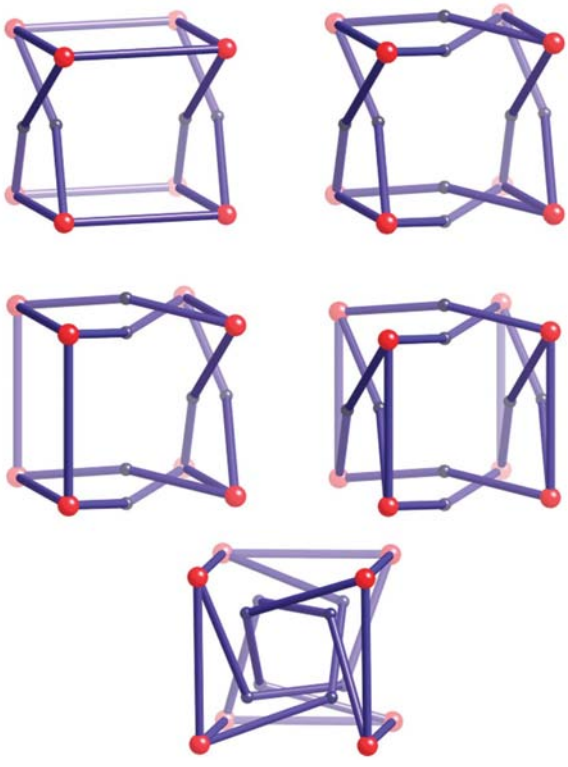

Figure 24
Embeddings of the knotted cubes with vertices located at the vertices of the standard (unknotted) Platonic cube.

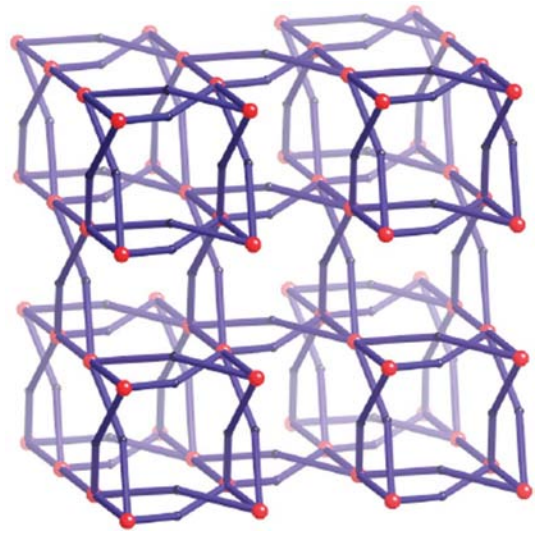

Figure 25
Body-centred tetragonal array of *B*-type cubes (with the *c* axis almost normal to the plane of the figure). Eight of the cubes edges are kinked (drawn with blue edges). The resulting structure consists of degree-six (red) vertices in a simple cubic arrangement.

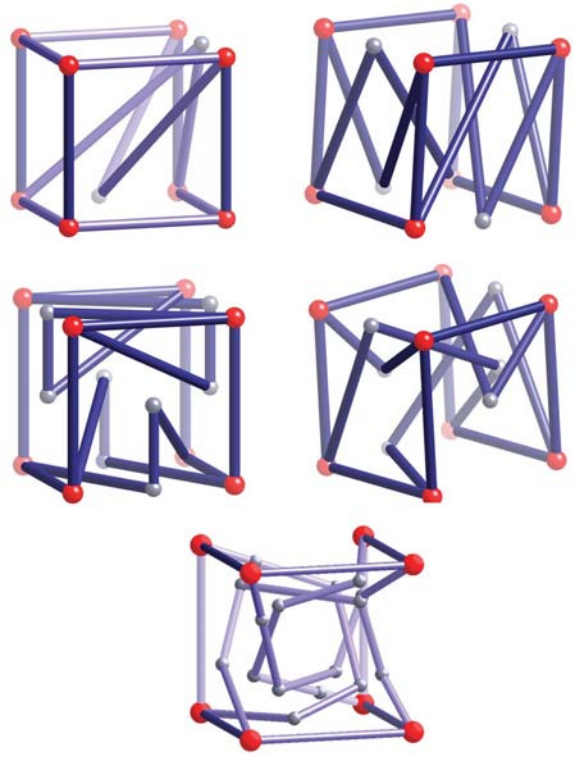

Figure 26
Embeddings of the knotted cubes with vertices located at the vertices of the standard (unknotted) Platonic cube and edges spanning vertex pairs in an identical form to those of the unknotted cube (in contrast to Fig. 24, where edges span vertices that are shuffled relative to the standard cube).

examples introduced above can be realized with straight edges, free of intersections, in $\mathbb{E}^3$. However, those embeddings require variations of edge lengths and vertex angles – unlike the usual embedding of the (unknotted) cube edges – giving asymmetric patterns. We can restore a measure of symmetry by allowing the edges to kink, to avoid intersections. Particularly appealing embeddings are afforded by locating the vertices so that they coincide with those of an unknotted Platonic cube. The resulting patterns all have non-trivial point groups, though their edges vary in length within a single isotope. Some of these patterns are shown in Fig. 24.

Recall that the unknotted simple cubic 'jungle-gym' network, pcu (O'Keeffe, 2003), results from vertex sharing of unknotted cubes arranged so that their centres lie on the sites of a body-centred lattice. We can substitute any of those cubes for any of the knotted examples shown in Fig. 24, to give knotted networks. A simple example, based on a body-centred (tetragonal) array of (*B*-type) wreath cubes with kinked edges is shown in Fig. 25. Numerous other examples can be envisaged, also based on body-centred arrangements. The most symmetric of those are realized by kinking or smoothly curving the edges, giving complex three-dimensional weavings, whose components are commonly double-helical fragments. Evidently, an infinity of tangled cubic nets are realizable *via* this operation. Generic examples are not isomorphic to the unknotted pcu net. However, if the tangled cubes are further tangled so that their edges span vertices in a manner identical to those of the unknotted cube, we are free to substitute these embeddings to give knotted varieties of the pcu framework. Cube embeddings that satisfy that condition are shown in Fig. 26.

Given the natural curvature of edges in relaxed versions of these tangled arrays, we do not expect to find them in atomic frameworks. However, the complex meandering bonds in metal-organic frameworks and polymeric crystals containing helical fragments may induce the formation of these mathematically rich structures.

We thank Davide Proserpio for discussions about knotted chemical frameworks. This particular project was inspired by the marvellous tangled polyhedral sculptures of Robert Owen. STH thanks Peter Harrowell for bringing them to his attention, Toen Castle for pointing out a missed example and Robert Owen for stimulating discussions. STH also acknowledges the Australian Research Council for financial support through a Federation Fellowship.

References

Adams, C. C. (2002). *The Knot Book*. New York: Henry Holt and Company.
Aste, T., Boose, D. & Rivier, N. (1996). *Phys. Rev. E*, **53**, 6181–6191.
Brinkmann, G. (1996). *J. Graph Theory*, **23**, 139–149.
Brunner, G. & Laves, F. (1971). *Wiss. Z. Techn. Univ. Dresden*, **20**, 387–390.
Carlucci, L., Ciani, G. & Proserpio, D. M. (2003*a*). *Coord. Chem. Rev.* **246**, 247–289.
Carlucci, L., Ciani, G. & Proserpio, D. M. (2003*b*). *CrystEngComm*, **5**, 269–279.
Castle, T., Robins, V. & Hyde, S. (2007). In preparation.
Cerf, C. (2002). *A family of impossible figures studied by knot theory*, http://www.mi.sanu.ac.yu/vismath/cerf/#r6.
Conder, M. & Dobsanyi, P. (2001). *J. Comb. Theory B*, **81**, 224–242.
Conway, J. & Gordon, C. (1983). *J. Graph Theory*, **7**, 445–453.
Conway, J. & Huson, D. (2002). *Struct. Chem.* **13**, 247–256.
Cowan, T. (1982). *J. Math. Psychol.* **26**, 252–262.
Coxeter, H. S. M. (1999). *The Beauty of Geometry: Twelve Essays*, *Angels and Devils*, pp. 197–209. New York: Dover Press.
Cromwell, P. R. (2001). *Polyhedra.* Cambridge University Press.
Delgado-Friedrichs, O., Foster, M. D., O'Keeffe, M., Proserpio, D. M., Treacy, M. M. J. & Yaghi, O. M. (2005). *J. Solid State Chem.* **178**, 2533–2554.
Delgado-Friedrichs, O. & O'Keeffe, M. (2003). *Acta Cryst.* A**59**, 351–360.
Delgado-Friedrichs, O. & O'Keeffe, M. (2005). *J. Solid State Chem.* **178**, 2480–2485.
Fischer, W. (2004). *Acta Cryst.* A**60**, 246–249.
Flapan, E. (2000). *When Topology Meets Chemistry.* Cambridge University Press.
Hyde, S., Delgado-Friedrichs, O., Ramsden, S. & Robins, V. (2006). *Solid State Sci.* **8**, 740–752.
Kauffman, L. H. (1989). *Trans. Am. Math. Soc.* **311**, 697–710.
Kepler, J. (1619). *Harmonice Mundi.*
Koch, E. & Sowa, H. (2004). *Acta Cryst.* A**60**, 239–245.
Lijnen, E. & Ceulemans, A. (2005). *J. Chem. Inf. Model*, **45**, 1719–1726.
Litherland, R. (1989). *Math. Proc. Camb. Philos. Soc.* **106**, 95–106.
McMullen, P. & Schulte, E. (1997). *Discrete Comput. Geom.* **17**, 449–478.
Moriuchi, H. (2004). *An enumeration of theta-curves with up to seven crossings*, http://knot.kaist.ac.kr/2004/proceedings/MORIUCHI.pdf.
O'Keeffe, M. (2003). *Reticular chemistry structural resource*, http://rcsr.anu.edu.au.
Owen, R. (2003). *Vessel #2* (blue second version), fibreglass and acrylic.
Plato (1965). *Timaeus.* Harmondsworth: Penguin. (Translated by H. D. P. Lee).
Ramsden, S., Hungerford, S., Hyde, S. & Robins, V. (2005). *Euclidean Patterns in Non-Euclidean Tilings*, http://epinet.anu.edu.au/.
Sauvage, J.-P. & Dietrich-Buchecker, C. (1999). *Catenanes, Rotaxanes and Knots.* New York: Wiley-VCH Verlag.
Seeman, N. & Lukeman, P. (2005). *Rep. Prog. Phys.* **68**, 237–270.
Simon, J. (1987). *J. Comput. Chem.* **8**, 718–726.
Stewart, B. M. (1970). *Adventures Among the Toroids. A Study of Quasi-Convex, Aplanar, Tunneled Orientable Polyhedra of Positive Genus having Regular Faces with Disjoint Interiors.* Michigan: B. M. Stewart.
Wolcott, K. (1987). In *Geometry and Topology: Manifolds, Varieties, and Knots*, edited by C. McCrory & T. Shifrin. New York: Marcel Dekker Inc.